

Study of Three-Body $\Upsilon(10860)$ Decays

I. Adachi,¹⁵ K. Adamczyk,⁴⁸ H. Aihara,⁷² K. Arinstein,³ Y. Arita,⁴¹ D. M. Asner,⁵⁴
T. Aso,⁷⁶ V. Aulchenko,³ T. Aushev,²⁷ T. Aziz,⁶⁷ A. M. Bakich,⁶⁶ Y. Ban,⁵⁶ E. Barberio,⁴⁰
M. Barrett,¹⁴ A. Bay,³⁵ I. Bedny,³ M. Belhorn,⁶ K. Belous,²⁴ V. Bhardwaj,⁴⁴ B. Bhuyan,¹⁹
M. Bischofberger,⁴⁴ S. Blyth,⁴⁶ A. Bondar,³ G. Bonvicini,⁷⁸ A. Bozek,⁴⁸ M. Bračko,^{38, 28}
J. Brodzicka,⁴⁸ O. Brovchenko,³⁰ T. E. Browder,¹⁴ M.-C. Chang,⁷ P. Chang,⁴⁷ Y. Chao,⁴⁷
V. Chekelian,³⁹ A. Chen,⁴⁵ K.-F. Chen,⁴⁷ P. Chen,⁴⁷ B. G. Cheon,¹³ K. Chilikin,²⁷
R. Chistov,²⁷ I.-S. Cho,⁸⁰ K. Cho,³¹ K.-S. Choi,⁸⁰ S.-K. Choi,¹² Y. Choi,⁶⁵ J. Crnkovic,¹⁸
J. Dalseno,^{39, 68} M. Danilov,²⁷ J. Dingfelder,² Z. Doležal,⁴ Z. Drásal,⁴ A. Drutskoy,²⁷
W. Dungel,²³ D. Dutta,¹⁹ S. Eidelman,³ D. Epifanov,³ S. Esen,⁶ J. E. Fast,⁵⁴ M. Feindt,³⁰
A. Frey,¹⁰ M. Fujikawa,⁴⁴ V. Gaur,⁶⁷ N. Gabyshev,³ A. Garmash,³ Y. M. Goh,¹³
B. Golob,^{36, 28} M. Grosse Perdekamp,^{18, 60} H. Guo,⁶² J. Haba,¹⁵ P. Hamer,¹⁰ Y. L. Han,²²
K. Hara,¹⁵ T. Hara,¹⁵ Y. Hasegawa,⁶⁴ K. Hayasaka,⁴² H. Hayashii,⁴⁴ D. Heffernan,⁵³
T. Higuchi,¹⁵ Y. Horii,⁴² Y. Hoshi,⁷⁰ K. Hoshina,⁷⁵ W.-S. Hou,⁴⁷ Y. B. Hsiung,⁴⁷
H. J. Hyun,³⁴ Y. Igarashi,¹⁵ T. Iijima,^{42, 41} M. Imamura,⁴¹ K. Inami,⁴¹ A. Ishikawa,⁷¹
R. Itoh,¹⁵ M. Iwabuchi,⁸⁰ M. Iwasaki,⁷² Y. Iwasaki,¹⁵ T. Iwashita,⁴⁴ S. Iwata,⁷⁴ I. Jaegle,¹⁴
M. Jones,¹⁴ T. Julius,⁴⁰ D. H. Kah,³⁴ H. Kakuno,⁷⁴ J. H. Kang,⁸⁰ P. Kapusta,⁴⁸
S. U. Kataoka,⁴³ N. Katayama,¹⁵ H. Kawai,⁵ T. Kawasaki,⁵⁰ H. Kichimi,¹⁵ C. Kiesling,³⁹
B. H. Kim,⁶³ H. J. Kim,³⁴ H. O. Kim,³⁴ J. B. Kim,³² J. H. Kim,³¹ K. T. Kim,³²
M. J. Kim,³⁴ S. K. Kim,⁶³ Y. J. Kim,³¹ K. Kinoshita,⁶ J. Klucar,²⁸ B. R. Ko,³²
N. Kobayashi,⁷³ S. Koblitz,³⁹ P. Kodyš,⁴ Y. Koga,⁴¹ S. Korpar,^{38, 28} R. T. Kouzes,⁵⁴
M. Kreps,³⁰ P. Križan,^{36, 28} P. Krokovny,³ B. Kronenbitter,³⁰ T. Kuhr,³⁰ R. Kumar,⁵⁵
T. Kumita,⁷⁴ E. Kurihara,⁵ Y. Kuroki,⁵³ A. Kuzmin,³ P. Kvasnička,⁴ Y.-J. Kwon,⁸⁰
S.-H. Kyeong,⁸⁰ J. S. Lange,⁸ M. J. Lee,⁶³ S.-H. Lee,³² M. Leitgab,^{18, 60} R. Leitner,⁴
J. Li,⁶³ X. Li,⁶³ Y. Li,⁷⁷ J. Libby,²⁰ C.-L. Lim,⁸⁰ A. Limosani,⁴⁰ C. Liu,⁶² Y. Liu,⁶
Z. Q. Liu,²² D. Liventsev,²⁷ R. Louvot,³⁵ J. MacNaughton,¹⁵ D. Marlow,⁵⁷ D. Matvienko,³
A. Matyja,⁴⁸ S. McOnie,⁶⁶ Y. Mikami,⁷¹ K. Miyabayashi,⁴⁴ Y. Miyachi,⁷⁹ H. Miyata,⁵⁰
Y. Miyazaki,⁴¹ R. Mizuk,²⁷ G. B. Mohanty,⁶⁷ D. Mohapatra,⁵⁴ A. Moll,^{39, 68} T. Mori,⁴¹
T. Müller,³⁰ N. Muramatsu,⁵⁸ R. Mussa,²⁶ T. Nagamine,⁷¹ Y. Nagasaka,¹⁶ Y. Nakahama,⁷²
I. Nakamura,¹⁵ E. Nakano,⁵² T. Nakano,⁵⁹ M. Nakao,¹⁵ H. Nakayama,¹⁵ H. Nakazawa,⁴⁵
Z. Natkaniec,⁴⁸ M. Nayak,²⁰ E. Nedelkovska,³⁹ K. Negishi,⁷¹ K. Neichi,⁷⁰ S. Neubauer,³⁰
C. Ng,⁷² M. Niiyama,³³ S. Nishida,¹⁵ K. Nishimura,¹⁴ O. Nitoh,⁷⁵ T. Nozaki,¹⁵ A. Ogawa,⁶⁰
S. Ogawa,⁶⁹ T. Ohshima,⁴¹ S. Okuno,²⁹ S. L. Olsen,^{63, 14} Y. Onuki,⁷² W. Ostrowicz,⁴⁸
H. Ozaki,¹⁵ P. Pakhlov,²⁷ G. Pakhlova,²⁷ H. Palka,⁴⁸ E. Panzenböck,^{10, 44} C. W. Park,⁶⁵
H. Park,³⁴ H. K. Park,³⁴ K. S. Park,⁶⁵ L. S. Peak,⁶⁶ T. K. Pedlar,³⁷ T. Peng,⁶²
R. Pestotnik,²⁸ M. Peters,¹⁴ M. Petrič,²⁸ L. E. Piilonen,⁷⁷ A. Poluektov,³ M. Prim,³⁰
K. Prothmann,^{39, 68} B. Reisert,³⁹ M. Ritter,³⁹ M. Röhrken,³⁰ J. Rorie,¹⁴ M. Rozanska,⁴⁸
S. Ryu,⁶³ H. Sahoo,¹⁴ K. Sakai,¹⁵ Y. Sakai,¹⁵ S. Sandilya,⁶⁷ D. Santel,⁶ L. Santelj,²⁸
T. Sanuki,⁷¹ N. Sasao,³³ Y. Sato,⁷¹ O. Schneider,³⁵ G. Schnell,^{1, 17} P. Schönmeier,⁷¹
C. Schwanda,²³ A. J. Schwartz,⁶ B. Schwenker,¹⁰ R. Seidl,⁶⁰ A. Sekiya,⁴⁴ K. Senyo,⁷⁹
O. Seon,⁴¹ M. E. Seviar,⁴⁰ L. Shang,²² M. Shapkin,²⁴ V. Shebalin,³ C. P. Shen,⁴¹

T.-A. Shibata,⁷³ H. Shibuya,⁶⁹ S. Shinomiya,⁵³ J.-G. Shiu,⁴⁷ B. Shwartz,³ A. Sibidanov,⁶⁶
 F. Simon,^{39,68} J. B. Singh,⁵⁵ R. Sinha,²⁵ P. Smerkol,²⁸ Y.-S. Sohn,⁸⁰ A. Sokolov,²⁴
 E. Solovieva,²⁷ S. Stanič,⁵¹ M. Starič,²⁸ J. Stypula,⁴⁸ S. Sugihara,⁷² A. Sugiyama,⁶¹
 M. Sumihama,⁹ K. Sumisawa,¹⁵ T. Sumiyoshi,⁷⁴ K. Suzuki,⁴¹ S. Suzuki,⁶¹ S. Y. Suzuki,¹⁵
 H. Takeichi,⁴¹ U. Tamponi,²⁶ M. Tanaka,¹⁵ S. Tanaka,¹⁵ K. Tanida,⁶³ N. Taniguchi,¹⁵
 G. Tatishvili,⁵⁴ G. N. Taylor,⁴⁰ Y. Teramoto,⁵² F. Thorne,²³ I. Tikhomirov,²⁷ K. Trabelsi,¹⁵
 Y. F. Tse,⁴⁰ T. Tsuboyama,¹⁵ M. Uchida,⁷³ T. Uchida,¹⁵ Y. Uchida,¹¹ S. Uehara,¹⁵
 K. Ueno,⁴⁷ T. Uglov,²⁷ Y. Unno,¹³ S. Uno,¹⁵ P. Urquijo,² Y. Ushiroda,¹⁵ Y. Usov,³
 S. E. Vahsen,¹⁴ P. Vanhoefer,³⁹ C. Van Hulse,¹ G. Varner,¹⁴ K. E. Varvell,⁶⁶ K. Vervink,³⁵
 A. Vinokurova,³ V. Vorobyev,³ A. Vossen,²¹ C. H. Wang,⁴⁶ J. Wang,⁵⁶ M.-Z. Wang,⁴⁷
 P. Wang,²² X. L. Wang,²² M. Watanabe,⁵⁰ Y. Watanabe,²⁹ R. Wedd,⁴⁰ E. White,⁶
 J. Wicht,¹⁵ L. Widhalm,²³ J. Wiechczynski,⁴⁸ K. M. Williams,⁷⁷ E. Won,³² B. D. Yabsley,⁶⁶
 H. Yamamoto,⁷¹ J. Yamaoka,¹⁴ Y. Yamashita,⁴⁹ M. Yamauchi,¹⁵ C. Z. Yuan,²² Y. Yusa,⁵⁰
 D. Zander,³⁰ C. C. Zhang,²² L. M. Zhang,⁶² Z. P. Zhang,⁶² L. Zhao,⁶² V. Zhilich,³
 P. Zhou,⁷⁸ V. Zhulanov,³ T. Zivko,²⁸ A. Zupanc,³⁰ N. Zwahlen,³⁵ and O. Zyukova³

(The Belle Collaboration)

¹*University of the Basque Country UPV/EHU, Bilbao*

²*University of Bonn, Bonn*

³*Budker Institute of Nuclear Physics SB RAS and
Novosibirsk State University, Novosibirsk 630090*

⁴*Faculty of Mathematics and Physics, Charles University, Prague*

⁵*Chiba University, Chiba*

⁶*University of Cincinnati, Cincinnati, Ohio 45221*

⁷*Department of Physics, Fu Jen Catholic University, Taipei*

⁸*Justus-Liebig-Universität Gießen, Gießen*

⁹*Gifu University, Gifu*

¹⁰*II. Physikalisches Institut, Georg-August-Universität Göttingen, Göttingen*

¹¹*The Graduate University for Advanced Studies, Hayama*

¹²*Gyeongsang National University, Chinju*

¹³*Hanyang University, Seoul*

¹⁴*University of Hawaii, Honolulu, Hawaii 96822*

¹⁵*High Energy Accelerator Research Organization (KEK), Tsukuba*

¹⁶*Hiroshima Institute of Technology, Hiroshima*

¹⁷*IKERBASQUE, Bilbao*

¹⁸*University of Illinois at Urbana-Champaign, Urbana, Illinois 61801*

¹⁹*Indian Institute of Technology Guwahati, Guwahati*

²⁰*Indian Institute of Technology Madras, Madras*

²¹*Indiana University, Bloomington, Indiana 47408*

²²*Institute of High Energy Physics,*

Chinese Academy of Sciences, Beijing

²³*Institute of High Energy Physics, Vienna*

²⁴*Institute of High Energy Physics, Protvino*

²⁵*Institute of Mathematical Sciences, Chennai*

²⁶*INFN - Sezione di Torino, Torino*

²⁷*Institute for Theoretical and Experimental Physics, Moscow*

- ²⁸*J. Stefan Institute, Ljubljana*
- ²⁹*Kanagawa University, Yokohama*
- ³⁰*Institut für Experimentelle Kernphysik,
Karlsruher Institut für Technologie, Karlsruhe*
- ³¹*Korea Institute of Science and Technology Information, Daejeon*
- ³²*Korea University, Seoul*
- ³³*Kyoto University, Kyoto*
- ³⁴*Kyungpook National University, Taegu*
- ³⁵*École Polytechnique Fédérale de Lausanne (EPFL), Lausanne*
- ³⁶*Faculty of Mathematics and Physics, University of Ljubljana, Ljubljana*
- ³⁷*Luther College, Decorah, Iowa 52101*
- ³⁸*University of Maribor, Maribor*
- ³⁹*Max-Planck-Institut für Physik, München*
- ⁴⁰*University of Melbourne, School of Physics, Victoria 3010*
- ⁴¹*Graduate School of Science, Nagoya University, Nagoya*
- ⁴²*Kobayashi-Maskawa Institute, Nagoya University, Nagoya*
- ⁴³*Nara University of Education, Nara*
- ⁴⁴*Nara Women's University, Nara*
- ⁴⁵*National Central University, Chung-li*
- ⁴⁶*National United University, Miao Li*
- ⁴⁷*Department of Physics, National Taiwan University, Taipei*
- ⁴⁸*H. Niewodniczanski Institute of Nuclear Physics, Krakow*
- ⁴⁹*Nippon Dental University, Niigata*
- ⁵⁰*Niigata University, Niigata*
- ⁵¹*University of Nova Gorica, Nova Gorica*
- ⁵²*Osaka City University, Osaka*
- ⁵³*Osaka University, Osaka*
- ⁵⁴*Pacific Northwest National Laboratory, Richland, Washington 99352*
- ⁵⁵*Panjab University, Chandigarh*
- ⁵⁶*Peking University, Beijing*
- ⁵⁷*Princeton University, Princeton, New Jersey 08544*
- ⁵⁸*Research Center for Electron Photon Science, Tohoku University, Sendai*
- ⁵⁹*Research Center for Nuclear Physics, Osaka University, Osaka*
- ⁶⁰*RIKEN BNL Research Center, Upton, New York 11973*
- ⁶¹*Saga University, Saga*
- ⁶²*University of Science and Technology of China, Hefei*
- ⁶³*Seoul National University, Seoul*
- ⁶⁴*Shinshu University, Nagano*
- ⁶⁵*Sungkyunkwan University, Suwon*
- ⁶⁶*School of Physics, University of Sydney, NSW 2006*
- ⁶⁷*Tata Institute of Fundamental Research, Mumbai*
- ⁶⁸*Excellence Cluster Universe, Technische Universität München, Garching*
- ⁶⁹*Toho University, Funabashi*
- ⁷⁰*Tohoku Gakuin University, Tagajo*
- ⁷¹*Tohoku University, Sendai*
- ⁷²*Department of Physics, University of Tokyo, Tokyo*
- ⁷³*Tokyo Institute of Technology, Tokyo*

⁷⁴*Tokyo Metropolitan University, Tokyo*

⁷⁵*Tokyo University of Agriculture and Technology, Tokyo*

⁷⁶*Toyama National College of Maritime Technology, Toyama*

⁷⁷*CNP, Virginia Polytechnic Institute and State University, Blacksburg, Virginia 24061*

⁷⁸*Wayne State University, Detroit, Michigan 48202*

⁷⁹*Yamagata University, Yamagata*

⁸⁰*Yonsei University, Seoul*

Abstract

We report preliminary results on the analysis of the three-body $\Upsilon(10860) \rightarrow B\bar{B}\pi$, $\Upsilon(10860) \rightarrow [B\bar{B}^* + \text{c.c.}]\pi$ and $\Upsilon(10860) \rightarrow B^*\bar{B}^*\pi$ decays including an observation of the $\Upsilon(10860) \rightarrow Z_b^\pm(10610)\pi^\mp \rightarrow [B\bar{B}^* + \text{c.c.}]^\pm\pi^\mp$ and $\Upsilon(10860) \rightarrow Z_b^\pm(10650)\pi^\mp \rightarrow [B^*\bar{B}^*]^\pm\pi^\mp$ decays as intermediate channels. We measure branching fractions of the three-body decays to be $\mathcal{B}(\Upsilon(10860) \rightarrow [B\bar{B}^* + \text{c.c.}]^\pm\pi^\mp) = (28.3 \pm 2.9 \pm 4.6) \times 10^{-3}$ and $\mathcal{B}(\Upsilon(10860) \rightarrow [B^*\bar{B}^*]^\pm\pi^\mp) = (14.1 \pm 1.9 \pm 2.4) \times 10^{-3}$ and set 90% C.L. upper limit $\mathcal{B}(\Upsilon(10860) \rightarrow [B\bar{B}]^\pm\pi^\mp) < 4.0 \times 10^{-3}$. We also report results on the amplitude analysis of the three-body $\Upsilon(10860) \rightarrow \Upsilon(nS)\pi^+\pi^-$, $n = 1, 2, 3$ decays and the analysis of the internal structure of the three-body $\Upsilon(10860) \rightarrow h_b(mP)\pi^+\pi^-$, $m = 1, 2$ decays. The results are based on a 121.4 fb^{-1} data sample collected with the Belle detector at a center-of-mass energy near the $\Upsilon(10860)$.

PACS numbers: 14.40.Pq, 13.25.Gv, 12.39.Pu

INTRODUCTION

Two new charged bottomonium-like resonances, $Z_b(10610)$ and $Z_b(10650)$, have recently been observed by the Belle Collaboration in decays of $\Upsilon(10860)$ to five different final states: $\Upsilon(nS)\pi^+\pi^-$, $n = 1, 2, 3$ and $h_b(mP)\pi^+\pi^-$, $m = 1, 2$ [1, 2]. The analysis of the quark composition of the initial and final states allows to assert that these hadronic objects are the first examples of states of an exotic nature: Z_b should be comprised of (at least) four quarks. Several models have been proposed to describe the internal structure of these states. One suggests [3] that $Z_b(10610)$ and $Z_b(10650)$ states might be a loosely bound $B\bar{B}^*$ and B^*B^* systems, respectively. The proximity of the $Z_b(10610)$ and $Z_b(10650)$ masses to those of the sum of the B and B^* mesons and the sum of the two B^* mesons, respectively, supports this hypothesis. In this case, it would be natural to expect that the $Z_b(10610)$ and $Z_b(10650)$ states decay respectively to $B\bar{B}^*$ and $B^*\bar{B}^*$ final states with substantial rates.

Evidence for the three-body $\Upsilon(10860) \rightarrow BB^*\pi$ decay has been previously reported by Belle in Ref. [4] with a data sample of 23.6 fb^{-1} . In this analysis we use 121.4 fb^{-1} of data accumulated by the Belle detector at a center-of-mass (c.m.) energy near the $\Upsilon(10860)$ to study three-body $\Upsilon(10860) \rightarrow [B^{(*)}\bar{B}^{(*)}]^\pm\pi^\mp$ decays and to search for $\Upsilon(10860) \rightarrow Z_b^\pm\pi^\mp \rightarrow [B^{(*)}\bar{B}^{(*)}]^\pm\pi^\mp$ decays.

Note that we reconstruct only three-body $B^{(*)}B^{(*)}\pi$ combinations with a charged primary pion. For brevity, we adopt the following notations: the sum of $B^+\bar{B}^0\pi^-$ and $B^-B^0\pi^+$ final states is referred to as $BB\pi$; the combination of $B^+\bar{B}^{*0}\pi^-$, $B^-B^{*0}\pi^+$, $B^0B^{*-}\pi^+$ and $\bar{B}^0B^{*+}\pi^-$ final states is referred to as $BB^*\pi$ and the sum of $B^{*+}\bar{B}^{*0}\pi^-$ and $B^{*-}B^{*0}\pi^+$ final states is denoted as $B^*B^*\pi$.

THE BELLE DETECTOR

The Belle detector [5] is located at the single interaction point of KEKB [6], an asymmetric energy double storage ring collider. The detector is a large-solid-angle magnetic spectrometer based on a 1.5 T superconducting solenoid magnet. Charged particle tracking is provided by a four-layer silicon vertex detector and a 50-layer central drift chamber (CDC) that surround the interaction point. The charged particle acceptance covers laboratory polar angles between $\theta = 17^\circ$ and 150° , corresponding to about 92% of the total solid angle in the c.m. frame.

Charged hadron identification is provided by dE/dx measurements in the CDC, an array of 1188 aerogel Cherenkov counters (ACC), and a barrel-like array of 128 time-of-flight scintillation counters (TOF); information from the three subdetectors is combined to form a single likelihood ratio, which is then used in kaon and pion selection. Electromagnetic showering particles are detected in an array of 8736 CsI(Tl) crystals (ECL) that covers the same solid angle as the charged particle tracking system. Electron identification in Belle is based on a combination of dE/dx measurements in the CDC, the response of the ACC, and the position, shape and total energy deposition (*i.e.*, E/p) of the shower detected in the ECL. The magnetic field is returned via an iron yoke that is instrumented to detect muons and K_L^0 mesons. We use a GEANT-based Monte Carlo (MC) simulation to model the response of the detector and determine its acceptance [7].

BACKGROUND SUPPRESSION

The dominant background comes from $e^+e^- \rightarrow c\bar{c}$ continuum events where real D mesons produced in e^+e^- annihilation are combined with random particles to form a B candidate. This type of background is suppressed using variables that characterize the event topology. Since the momenta of two B mesons produced from a three-body $\Upsilon(10860)$ decay are low in the c.m. frame, their decay products are essentially uncorrelated and the event tends to be spherical. In contrast, hadrons from continuum events tend to exhibit a two-jet structure. We use θ_{thr} , the angle between the thrust axis of the B candidate and that of the rest of the event, to discriminate between the two cases. The distribution of $|\cos\theta_{\text{thr}}|$ is strongly peaked near $|\cos\theta_{\text{thr}}| = 1.0$ for $c\bar{c}$ events and is nearly flat for $B^{(*)}B^{(*)}\pi$ events. We require $|\cos\theta_{\text{thr}}| < 0.80$ for $B \rightarrow D^{(*)}\pi$ final states; this eliminates about 81% of the continuum background and retains 73% of the signal events.

Another significant background comes from events with radiative return to a lower mass $\Upsilon(4S)$ state with a subsequent $\Upsilon(4S) \rightarrow B\bar{B}$ decay. Momenta of B mesons produced in this process fall in the same region as those for B mesons from the three-body $\Upsilon(10860) \rightarrow B^{(*)}B^{(*)}\pi$ decays. B mesons originating from the two-body $\Upsilon(10860) \rightarrow B^*B^*$, BB^* , BB decays produce peaks around $P(B) = 1.07$ GeV/ c , 1.18 GeV/ c and 1.28 GeV/ c , respectively. Momenta of B mesons from three-body $\Upsilon(10860) \rightarrow B^{(*)}B^{(*)}\pi$ decays are less than 0.9 GeV/ c .

EVENT RECONSTRUCTION

Charged tracks are selected with a set of track quality requirements based on the number of CDC hits and on the distances of closest approach to the interaction point (IP). Tracks originated from B candidate are required to have momenta transverse to the beam be greater than 0.1 GeV/ c to reduce the low momentum combinatorial background. For charged kaon identification, we impose a requirement on the particle identification variable, which has 86% efficiency and a 7% fake rate from misidentified pions. Charged tracks that are positively identified as electrons or protons are excluded. Since the muon identification efficiency and fake rate vary significantly with the track momentum, we do not veto muons to avoid additional systematic errors.

Photons from neutral pions are required to produce clusters in the ECL with an energy deposition of greater than 50 MeV and not be associated with charged tracks. The invariant mass of the two-photon combination is required to be within 12 MeV/ c^2 of the nominal π^0 mass. The K^{*0} is reconstructed in the $K^{*0} \rightarrow K^+\pi^-$ mode, the invariant mass of the K^{*0} candidate is required to be within 70 MeV/ c^2 of the nominal K^{*0} mass. The invariant mass of the $J/\psi \rightarrow \mu^+\mu^-$ candidates is required to satisfy $|M(\mu^+\mu^-) - M_{J/\psi}| < 30$ MeV/ c^2 , where $M_{J/\psi}$ is the nominal mass of the J/ψ meson. Neutral (charged) D mesons originating from B decays are reconstructed in the $\bar{D}^0 \rightarrow K^+\pi^-$ and $\bar{D}^0 \rightarrow K^+\pi^+\pi^-\pi^-$ ($D^- \rightarrow K^+\pi^-\pi^-$) modes. Those originating from D^{*-} decays are also reconstructed in the $\bar{D}^0 \rightarrow K^+\pi^-\pi^0$ mode. To identify D^{*-} candidates we require $|M(\bar{D}^0\pi^-) - M(\bar{D}^0) - \Delta M_D| < 2$ MeV/ c^2 , where $M(\bar{D}^0)$ and $M(\bar{D}^0\pi^-)$ are the reconstructed masses of the D^0 candidate and $D^0\pi^-$ system, respectively, and $\Delta M_D = M_{D^*} - M_D$.

B decays are reconstructed in the following channels: $B^+ \rightarrow J/\psi K^+$, $B^+ \rightarrow \bar{D}^0\pi^+$, $B^0 \rightarrow J/\psi K^{*0}$, $B^0 \rightarrow D^-\pi^+$, $B^0 \rightarrow D^{*-}\pi^+$. We identify B candidates by their invariant mass $M(B)$ and momentum $P(B)$. $M(B)$ and $P(B)$ distributions for B candidates in

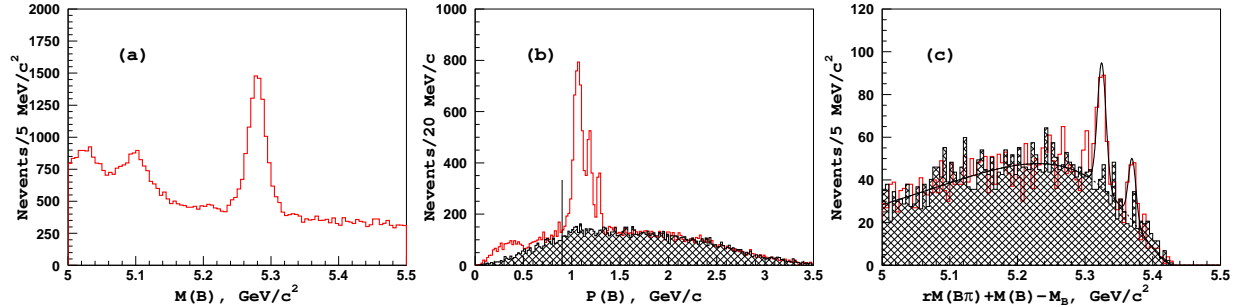


FIG. 1: (a) Invariant mass, (b) momentum and (c) $M_r(B\pi)$ distributions for selected B candidates in data. Hatched histograms in (b) and (c) show distributions for events in $M(B)$ sidebands.

data are shown in Figs. 1(a) and 1(b). We require $M(B)$ to be within 30 to 40 MeV/c^2 (depending on the B decay mode) of the nominal B mass. Mass sidebands are defined as $50 \text{ MeV}/c^2 < |M(B) - M_B| < 80 \text{ MeV}/c^2$.

Reconstructed B^+ or B^0 candidates are then combined with a π^- candidate and a recoil mass to the $B\pi$ combination, $M_r(B\pi)$, is calculated as $M_r(B\pi) = \sqrt{E_{\text{cms}}^2 - P_{B\pi}^2}$, where E_{cms} is the c.m. energy and $P_{B\pi}$ is the measured three-momentum of the $B\pi$ combination. Signal $\Upsilon(10860) \rightarrow BB^*\pi$ events produce a narrow peak in the $M_r(B\pi)$ spectrum around the nominal B^* mass, while $\Upsilon(10860) \rightarrow B^*B^*\pi$ events produce a peak shifted to higher mass by about $45 \text{ MeV}/c^2$ due to a missed photon from the $B^* \rightarrow B\gamma$ decay. It is important to note here that, according to signal MC, $BB^*\pi$ events where the reconstructed B is the one from B^* produce a peak in the $M_r(B\pi)$ distribution at virtually the same position as $BB^*\pi$ events, where the reconstructed B is the prompt one. To remove a correlation between $M_r(B\pi)$ and $M(B)$ and to improve the resolution, we use $M_r(B\pi) + M(B) - M_B$ instead of $M_r(B\pi)$. The $M_r(B\pi) + M(B) - M_B$ distribution for experimental data is shown in Figure 1(c), where clear peaks are visible in the $BB^*\pi$ and $B^*B^*\pi$ signal regions.

To determine the distribution of background events we combine a reconstructed B candidate with pions of the wrong charge. The $M_r(B\pi) + M(B) - M_B$ distribution for wrong-sign combinations is shown as a hatched histogram in Fig. 1(c). While wrong-sign $B\pi$ combinations reproduce the shape of the combinatorial background very well, the amount of the background is underestimated by about 18%. To correct for this effect, we introduce a scale factor of 1.18 for wrong-sign combinations; the $M_r(B\pi)$ distributions shown in Fig. 1(c) include this correction factor. The resolution of the signal peaks in Fig. 1(c) is fixed at $6.1 \text{ MeV}/c^2$ as determined from signal MC.

ANALYSIS OF $\Upsilon(10860) \rightarrow [B^{(*)}B^*]\mp\pi^\pm$

The fit to the $M_r(B\pi) + M(B) - M_B$ distribution for signal events shown in Fig. 1(c) yields $N_{BB^*\pi} = 1 \pm 14$, $N_{B^*B^*\pi} = 184 \pm 19$ and $N_{B^*B^*\pi} = 82 \pm 11$ signal events. The statistical significance of the observed $BB^*\pi$ and $B^*B^*\pi$ signal is 9.3σ and 5.7σ , respectively. The statistical significance here is calculated as $\sqrt{-2 \ln(\mathcal{L}_0/\mathcal{L}_{\text{sig}})}$, where \mathcal{L}_{sig} and \mathcal{L}_0 denote the likelihood values obtained with the nominal fit and with the signal yield fixed at zero, respectively.

For the subsequent analysis of the internal structures of the three-body decays, we require

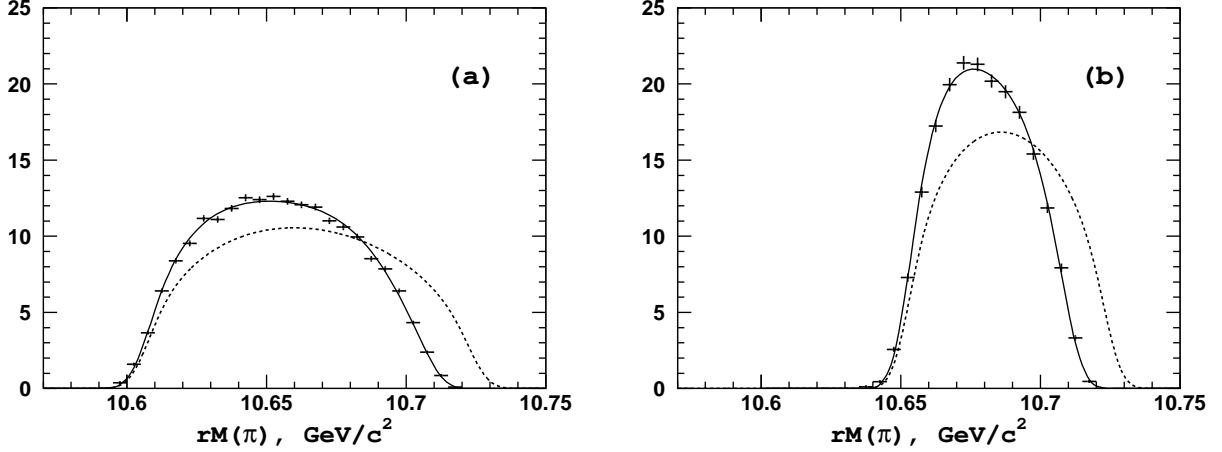


FIG. 2: PDFs for reconstruction efficiency for the (a) $\Upsilon(10860) \rightarrow BB^*\pi$ and (b) $\Upsilon(10860) \rightarrow B^*B^*\pi$ signals. Points with error bars show signal MC with the phase-space distribution of signal events, the solid line is the result of the fit, and the dashed line is the phase space with uniform efficiency.

$|(M_r(B) + M(B) - M_B) - M_{B^*}| < 0.015 \text{ GeV}/c^2$ to select $\Upsilon(10860) \rightarrow BB^*\pi$ events and $|(M_r(B) + M(B) - M_B) - (M_{B^*} + E_\gamma)| < 0.015 \text{ GeV}/c^2$, where $E_\gamma = 0.049 \text{ GeV}$ [8], to select $\Upsilon(10860) \rightarrow B^*B^*\pi$ events. For selected $B^{(*)}B^{(*)}\pi$ candidate events, we calculate the mass recoiling against the charged pion: $M_r(\pi) = \sqrt{E_{\text{cms}}^2 - P_\pi^2}$, where $P_{B\pi}$ is the measured three-momentum of the charged pion. The $M_r(\pi)$ distributions for signal $\Upsilon(10860) \rightarrow BB^*\pi$ and $\Upsilon(10860) \rightarrow B^*B^*\pi$ MC events generated with the uniform phase space distribution are shown in Fig. 2. To parameterize the $M_r(\pi)$ dependence of the reconstruction efficiency $E_{BB^*\pi}(m)$, we use the following empirical function:

$$E_{B^{(*)}B^{(*)}\pi}(m) = a_0(1 + a_1\delta_m + a_2\delta_m^2 + a_3\delta_m^3 + a_4\delta_m^4) \times \text{PHSP}_{B^{(*)}B^{(*)}\pi}(m), \quad (1)$$

where $m \equiv M_r(\pi)$, $\delta_m = m - m_0$, $m_0 = M_{B^{(*)}} + M_{B^*}$ and a_i are fit parameters, and $\text{PHSP}(m)$ is the phase space function for the $\Upsilon(10860) \rightarrow B^{(*)}B^{(*)}\pi$ decay. To account for the instrumental resolution, we smear the efficiency given by Eq. (1) with a Gaussian function. The resolution σ_m of the Gaussian is dominated by the c.m. energy spread and fixed to be $\sigma_m = 6 \text{ MeV}/c^2$. The results of the fit are shown in Fig. 2.

The $M_r(\pi)$ distributions for wrong-sign $B\pi$ combinations for events in the $BB^*\pi$ and $B^*B^*\pi$ signal regions are shown in Fig. 3. We use the following empirical function to parameterize the distribution of background events

$$B_{B^{(*)}B^*\pi}(m) = b_0 e^{-\alpha\delta_m} \times E_{B^{(*)}B^*\pi}(m), \quad (2)$$

where b_0 and α are fit parameters. As in the case of the fit to the efficiency PDF, the background PDF is convolved with a resolution function. Results of fits to sideband events are shown in Fig. 3.

The $M_r(\pi)$ distributions for right-sign $B\pi$ combinations in the $BB^*\pi$ and $B^*B^*\pi$ signal regions are shown in Fig. 4. Excesses of signal events over the expected background levels at lower mass edges of the $M_r(\pi)$ spectra are clearly visible for both final states. The distribution of signal $\Upsilon(10860) \rightarrow BB^*\pi$ events is parameterized with the following model

$$S_{BB^*\pi}(m) = (A_{Z_b(10610)} + A_{NR}) \times E_{BB^*\pi}(m), \quad (3)$$

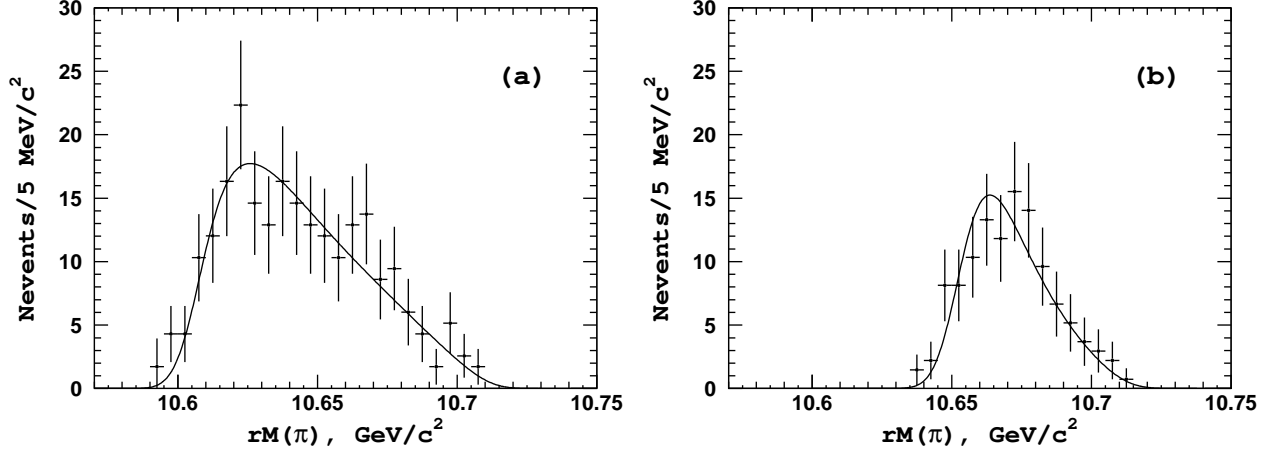


FIG. 3: $M_r(\pi)$ distribution for wrong-sign $B\pi$ combinations for the (a) $BB^*\pi$ and (b) $B^*B^*\pi$ candidate events. Points with error bars are data, the solid line is the result of the fit with a function of Eq.(2).

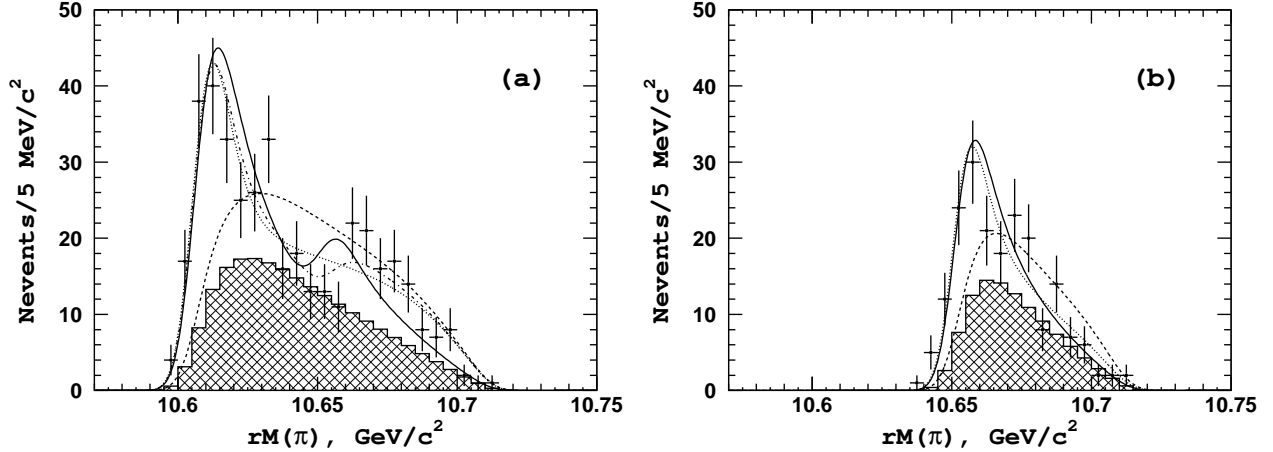


FIG. 4: $M_r(\pi)$ distribution for right-sign $B\pi$ combinations for (a) $\Upsilon(10860) \rightarrow BB^*\pi$ and (b) $\Upsilon(10860) \rightarrow B^*B^*\pi$ candidate events. Points with error bars are data, the solid line is the result of the fit with the nominal model (see text), the dashed line - fit to pure non-resonant amplitude, the dotted line - fit to a single Z_b state plus a non-resonant amplitude, and the dash-dotted - two Z_b states and a non-resonant amplitude. The hatched histogram represents background component normalized to the estimated number of background events.

where A_{NR} is the non-resonant amplitude parameterized as a complex constant and the $Z_b(10610)$ amplitude is a Breit-Wigner function. As a variation of this nominal model, we also add a second Breit-Wigner amplitude to account for possible $Z_b(10650) \rightarrow BB^*\pi$ decay. We also fit the data with only the $Z_b(10610)$ channel included in the decay amplitude. The results of these fits are shown in Fig. 4(a). Two models give about equally good description of the data: nominal model and a model with additional non-resonant amplitude. However, we select the former one as our nominal model since adding a non-resonant amplitude does

TABLE I: Summary of fit results to the $M_r(\pi)$ distribution for three-body $\Upsilon(10860) \rightarrow BB^*\pi$ and $\Upsilon(10860) \rightarrow B^*B^*\pi$ decays.

Mode	Parameter	Nominal model	Model-1	Model-2	Model-3	Model-4
$BB^*\pi$	$f_{Z_b(10610)}$	1.08 ± 0.12	–	0.86 ± 0.15	1.0	0.73 ± 0.17
	$f_{Z_b(10650)}$	0.25 ± 0.10	–	–	–	0.087 ± 0.061
	$\phi_{Z_b(10650)}$	-0.93 ± 0.34	–	–	–	0.32 ± 0.23
	f_{NR}	–	1.0	1.37 ± 0.28	–	1.17 ± 0.27
	ϕ_{NR}	–	–	0.18 ± 0.21	–	2.75 ± 1.03
	$-\log \mathcal{L}$	142	226	129	162	126
$B^*B^*\pi$	$f_{Z_b(10650)}$	1.0	–	0.83 ± 0.14		
	f_{NR}	–	1.0	0.78 ± 0.43		
	ϕ_{NR}	–	–	0.53 ± 2.4		
	$-\log \mathcal{L}$	86.0	133.6	83.6		

not improve the fit quality that much. The worst fit to the data is provided by a model with just a non-resonant amplitude. From this analysis, we estimate that the significance of the $Z_b(10610) \rightarrow BB^*$ signal exceeds the 8σ level.

As the nominal model for the $\Upsilon(10860) \rightarrow B^*B^*\pi$ decay, we use the following parameterization:

$$S_{B^*B^*\pi}(m) = (A_{Z_b(10650)} + A_{NR})E_{B^*B^*\pi}(m). \quad (4)$$

We also fit the data without a non-resonant component and with a non-resonant amplitude alone. Results of the fits are shown in Fig. 4(b); numerical values are given in Table I.

The best description of the $B^*B^*\pi$ data is achieved in a model with only the $Z_b(10650)$ amplitude included. The addition of a non-resonant amplitude does not provide any significant improvement of the fit quality. The fit with a non-resonant amplitude alone gives a much worse likelihood value. From this analysis, we determine the significance of the $Z_b(10650) \rightarrow B^*B^*$ signal to be 6.8σ .

In all fits discussed above, the masses and widths of the Z_b states were fixed at the values obtained from the analysis of the $\Upsilon(nS)\pi^+\pi^-$ and $h_b(mP)\pi^+\pi^-$ final states: $M[Z_b(10610)] = 10607.2 \pm 2.0$ MeV/ c^2 , $\Gamma[Z_b(10610)] = 18.4 \pm 2.4$ MeV and $M[Z_b(10650)] = 10652.2 \pm 1.5$ MeV/ c^2 , $\Gamma[Z_b(10650)] = 11.5 \pm 2.2$ MeV. If allowed to float, the fit returns 10597 ± 9 MeV for $Z_b(10610)$ mass in the fit to $BB^*\pi$ events and 10649 ± 12 MeV for $Z_b(10650)$ mass in the fit to $B^*B^*\pi$ events. Large errors here reflect a strong negative correlation between resonance mass and its amplitude.

ANALYSIS OF $\Upsilon(10860) \rightarrow \Upsilon(nS)\pi^+\pi^-$

In addition to new results on the analysis of the three-body $\Upsilon(10860) \rightarrow B^{(*)}B^{(*)}\pi$ decays described in previous sections, we extend our analysis of the three-body $\Upsilon(10860) \rightarrow \Upsilon(nS)\pi^+\pi^-$ and $\Upsilon(10860) \rightarrow h_b(mP)\pi^+\pi^-$ decays reported earlier in Ref. [1] to measure not only the parameters of the newly observed Z_b states but also the fractions of individual components contributing to the three-body signals.

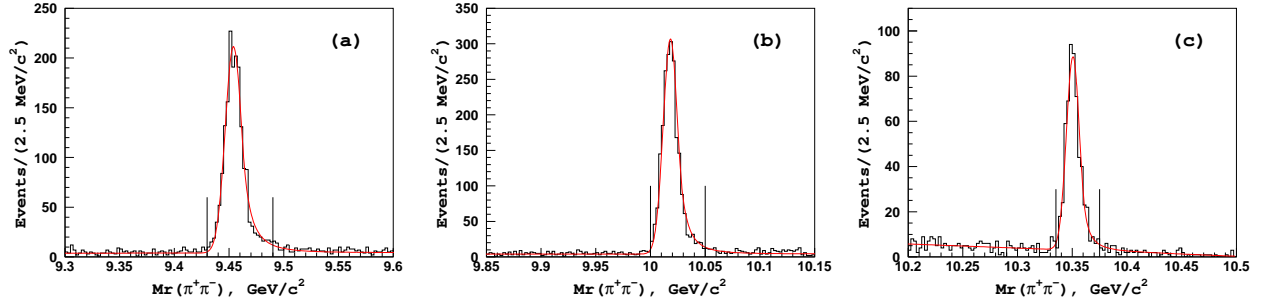


FIG. 5: Distribution of recoil mass associated with the $\pi^+\pi^-$ combination for $\Upsilon(5S) \rightarrow \Upsilon(nS)\pi^+\pi^-$ candidate events in the (a) $\Upsilon(1S)$; (b) $\Upsilon(2S)$; (c) $\Upsilon(3S)$ mass region. Vertical lines define the corresponding signal region.

To select $\Upsilon(10860) \rightarrow \Upsilon(nS)\pi^+\pi^-$ ($n = 1, 2, 3$) candidate events, we require the presence of a pair of muon candidates with an invariant mass in the range of $8.0 \text{ GeV}/c^2 < M(\mu^+\mu^-) < 11.0 \text{ GeV}/c^2$ and two pion candidates of opposite charge in the event. All tracks are required to originate from the vicinity of the interaction point. We also require that none of the four tracks be consistent with being an electron. More details on the analysis flow can be found in Ref. [1] and references therein.

Candidate $\Upsilon(10860) \rightarrow \Upsilon(nS)\pi^+\pi^-$ events are identified via the measured invariant mass of the $\mu^+\mu^-$ combination and the recoil mass, $M_r(\pi^+\pi^-)$, associated with the $\pi^+\pi^-$ system calculated as $M_r(\pi^+\pi^-) \equiv \sqrt{(E_{\text{c.m.}} - E_{\pi^+\pi^-}^*)^2 - p_{\pi^+\pi^-}^{*2}}$, where $E_{\pi^+\pi^-}$ and $p_{\pi^+\pi^-}^*$ are the energy and momentum of the $\pi^+\pi^-$ system measured in the c.m. frame. Events originating from $\Upsilon(10860)$ decays are selected with the requirement of $|M_r(\pi^+\pi^-) - M(\mu^+\mu^-)| < 0.2 \text{ GeV}/c^2$. The $M_r(\pi^+\pi^-)$ distributions shown in Fig. 5 are fit to the sum of a Crystal Ball function for the $\Upsilon(nS)$ signal and a linear function for the combinatorial background component. Results of the fits are shown in Fig. 5.

For the subsequent analysis, we select events around a respective $\Upsilon(nS)$ mass peak as shown in Fig. 5. After all the selections are applied, we come up with 1819, 2219 and 588 events for the $\Upsilon(1S)\pi^+\pi^-$, $\Upsilon(2S)\pi^+\pi^-$ and $\Upsilon(3S)\pi^+\pi^-$ final state, respectively. The fractions of signal events in the selected samples are determined from the fit to the corresponding $M_r(\pi^+\pi^-)$ spectrum.

The amplitude analysis of three-body $\Upsilon(10860) \rightarrow \Upsilon(nS)\pi^+\pi^-$ ($n = 1, 2, 3$) decays is performed by means of an unbinned maximum likelihood fit. The distribution of background events is determined using events in the $\Upsilon(nS)$ mass sidebands. The variation of reconstruction efficiency over the phase space is determined using MC simulated signal events generated with a uniform distribution.

We use the following parameterization of the $\Upsilon(10860) \rightarrow \Upsilon(nS)\pi^+\pi^-$ three-body decay amplitude:

$$M(s_1, s_2) = A_1(s_1, s_2) + A_2(s_1, s_2) + A_{f_0} + A_{f_2} + A_{NR},$$

where $s_1 = m^2(Y(nS)\pi^+)$, $s_2 = m^2(Y(nS)\pi^-)$. The amplitudes A_1 and A_2 are S -wave Breit-Wigner functions to account for the observed $Z_b(10610)$ and $Z_b(10650)$ peaks, respectively. To account for the possibility for the $\Upsilon(10860)$ to decay to both $Z^+\pi^-$ and $Z^-\pi^+$ channels, the amplitudes A_1 and A_2 are symmetrized with respect to π^+ and π^- interchange. Taking into account isospin symmetry, the resulting amplitude is written as

$$A_k = a_k e^{i\delta_k} (BW(s_1, m_k, \Gamma_k) + BW(s_2, m_k, \Gamma_k)),$$

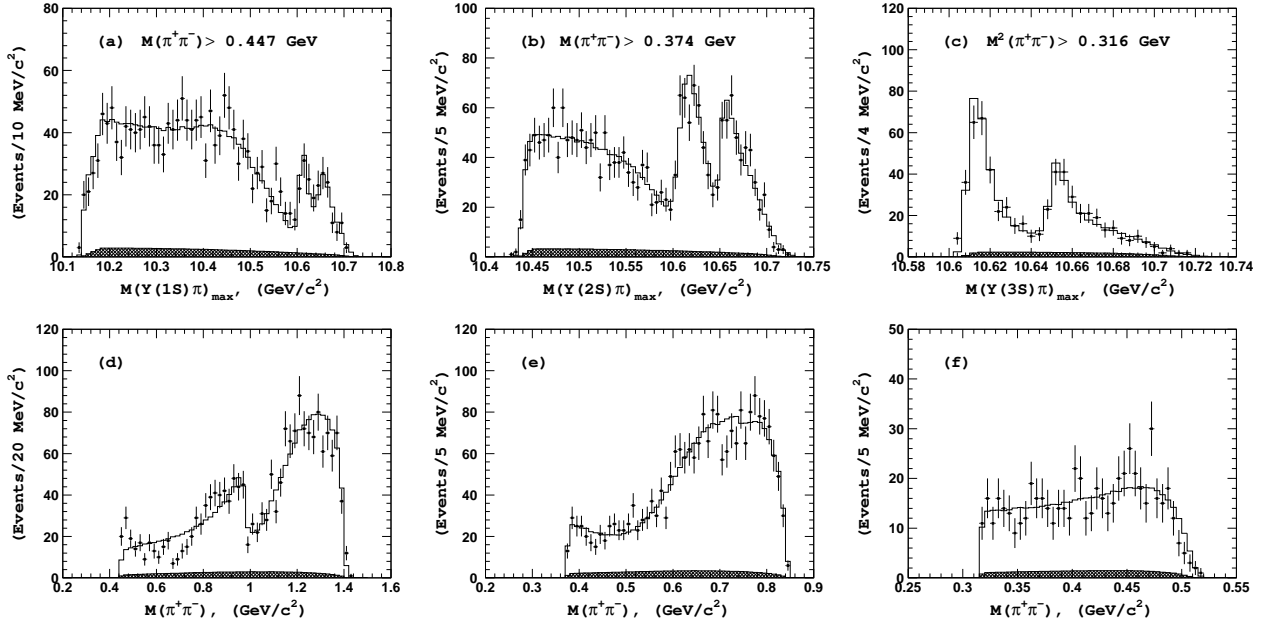


FIG. 6: Comparison of fit results (open histogram) with experimental data (points with error bars) for $\Upsilon(1S)\pi^+\pi^-$ events (left column), $\Upsilon(2S)\pi^+\pi^-$ events (middle column) and $\Upsilon(3S)\pi^+\pi^-$ events (right column) in the signal region. The hatched histograms show the background component.

where the masses m_k and widths Γ_k ($k = 1, 2$) are free parameters of the fit. Due to the very limited phase space available in $\Upsilon(10860) \rightarrow \Upsilon(nS)\pi^+\pi^-$ decays, $\Upsilon(10860) \rightarrow Z_b^+\pi^-$ and $\Upsilon(10860) \rightarrow Z_b^-\pi^+$ amplitudes overlap significantly. We also include amplitudes A_{f_0} and A_{f_2} to account for possible contributions from $f_0(980)$ scalar and $f_2(1270)$ tensor states. We use a Breit-Wigner function to parameterize the $f_2(1270)$ and a Flatté function for the $f_0(980)$. The mass and width of the $f_2(1270)$ state are fixed at their world average values [8]; the mass and coupling constants of the $f_0(980)$ state are fixed at the values defined from the analysis of $B^+ \rightarrow K^+\pi^+\pi^-$: $M(f_0(980)) = 950 \text{ MeV}/c^2$, $g_{\pi\pi} = 0.23$, $g_{KK} = 0.73$ [10].

Following the suggestion given in Refs.[11, 12], the non-resonant amplitude A_{NR} is parameterized as

$$A_{NR} = a \cdot e^{i\delta_1^{\text{nr}}} + b \cdot e^{i\delta_2^{\text{nr}}} \cdot s_3,$$

where $s_3 = m^2(\pi^+\pi^-)$, a_{nr} , b_{nr} , δ_1^{nr} and δ_2^{nr} are free parameters of the fit (s_3 is not an independent variable and can be expressed via s_1 and s_2 but we prefer to keep it here for simplicity).

The logarithmic likelihood function \mathcal{L} is then constructed as

$$\mathcal{L} = -2 \sum \log(f_{\text{sig}}S(s_1, s_2) + (1 - f_{\text{sig}})B(s_1, s_2)),$$

where $S(s_1, s_2)$ is formed from $|M(s_1, s_2)|^2$ convolved with the detector resolution and f_{sig} is the fraction of signal events in the data sample. Results of fits to $\Upsilon(10860) \rightarrow \Upsilon(nS)\pi^+\pi^-$ signal events are shown in Fig. 6, where one-dimensional projections of the data and fits are presented.

Results on the Z_b parameters are reported in Ref. [1]. Here, we report fractions of intermediate channels contributing to each three-body final state. The results are summarized in

TABLE II: Summary of results on fractions of individual quasi-two-body channels contributing to $\Upsilon(10860) \rightarrow \Upsilon(nS)\pi^+\pi^-$ three-body decays.

Final state	$\Upsilon(1S)\pi^+\pi^-$	$\Upsilon(2S)\pi^+\pi^-$	$\Upsilon(3S)\pi^+\pi^-$
$\mathcal{B}(Z_b^\mp(10610)\pi^\pm) \times \mathcal{B}(Z_b^\mp(10610) \rightarrow \Upsilon(nS)\pi^\pm)$, %	$2.54_{-0.51-0.55}^{+0.86+0.13}$	$19.6_{-3.1-0.6}^{+3.5+1.9}$	$26.8_{-3.9}^{+6.6} \pm 1.5$
$\mathcal{B}(Z_b^\mp(10650)\pi^\pm) \times \mathcal{B}(Z_b^\mp(10650) \rightarrow \Upsilon(nS)\pi^\pm)$, %	$1.04_{-0.31-0.12}^{+0.65+0.07}$	$5.77_{-0.96-1.56}^{+1.44+0.27}$	$11.0_{-2.3}^{+4.2} \pm 0.7$
$\mathcal{B}(\Upsilon(nS)f_2(1270)) \times \mathcal{B}(f_2(1270) \rightarrow \pi^+\pi^-)$, %	$15.6 \pm 1.4 \pm 2.1$	$2.81_{-0.56-0.86}^{+0.84+0.63}$	—
Total S -wave, %	$89.2 \pm 3.0 \pm 2.4$	$105.6 \pm 4.1 \pm 2.6$	$45.6 \pm 5.3 \pm 0.8$

Table IV, where the central values are determined from fits with the nominal model. Statistical uncertainties are determined from fits to multiple toy MC samples generated according to the nominal model. This allows us to account for correlations between various channels. In general, we find that all the three-body $\Upsilon(10860) \rightarrow \Upsilon(nS)\pi^+\pi^-$ decays are dominated by the S -wave channels with some statistically significant D -wave contribution.

The dominant systematic uncertainty in the fractions of individual channels contributing to three-body decays comes from the model uncertainty. We estimate this uncertainty by fitting the signal with various modifications of the nominal model. For example, we vary the parameterization of the non-resonant amplitude or replace the $\Upsilon(nS)f_2(1270)$ amplitude with a D -wave non-resonant component.

ANALYSIS OF $\Upsilon(10860) \rightarrow h_b(mP)\pi^+\pi^-$

In the analysis of the $\Upsilon(10860) \rightarrow h_b(mP)\pi^+\pi^-$ decays, we perform an inclusive reconstruction of signal events utilizing the recoil mass, $M_r(\pi^+\pi^-)$, associated with a $\pi^+\pi^-$ pair. The selection requirements are identical to those described in Ref. [2]. The continuum $e^+e^- \rightarrow q\bar{q}$ ($q = u, d, s, c$) background is suppressed by a requirement on the ratio of the second to zeroth Fox-Wolfram moments $R_2 < 0.3$ [14]. We select π^\pm candidates that originate from the vicinity of the interaction point and are positively identified as pions based on the CDC (dE/dx), TOF and ACC information. We reject tracks that are identified as electrons.

Because of the extremely high combinatorial background, a Dalitz analysis of the $\Upsilon(10860) \rightarrow h_b(mP)\pi^+\pi^-$ decay is challenging. Instead, we study the one-dimensional projection by fitting the $M_r(\pi^+\pi^-)$ spectra in bins of the $h_b(1P)\pi^\pm$ mass. We define the $h_b(1P)\pi^\pm$ mass as the recoil mass, $M_r(\pi^\mp)$, associated with a single charged pion. We symmetrize the distributions by combining the $M_r(\pi^+\pi^-)$ spectra corresponding to $M_r(\pi^+)$ and $M_r(\pi^-)$ bins and restrict the analysis to the $M_r(\pi) > 10.40 \text{ GeV}/c^2$ ($M_r(\pi) > 10.57 \text{ GeV}/c^2$) region for the $h_b(1P)\pi^+\pi^-$ ($h_b(2P)\pi^+\pi^-$) final state to avoid double counting. Each $M_r(\pi^+\pi^-)$ spectrum is fit to extract the $h_b(1P)$ and the $h_b(2P)$ signal yields. The fitting function is a sum of a Crystal Ball function for the $h_b(mP)$ signal and a Chebyshev polynomial for the combinatorial background. We also account for the $\Upsilon(2S)$ signal and a reflection from $\Upsilon(3S) \rightarrow \Upsilon(1S)\pi^+\pi^-$ decay. Details of this analysis can be found in Ref. [2]. The $h_b(mP)$ yields as a function of the $M_r(\pi^\mp)$ are shown in Fig. 7, where a clear two-peak structure is apparent for both $h_b(1P)\pi^+\pi^-$ and $h_b(2P)\pi^+\pi^-$ final states.

We perform a χ^2 fit of the $M_r(\pi)$ distributions to a coherent sum of two P -wave Breit-

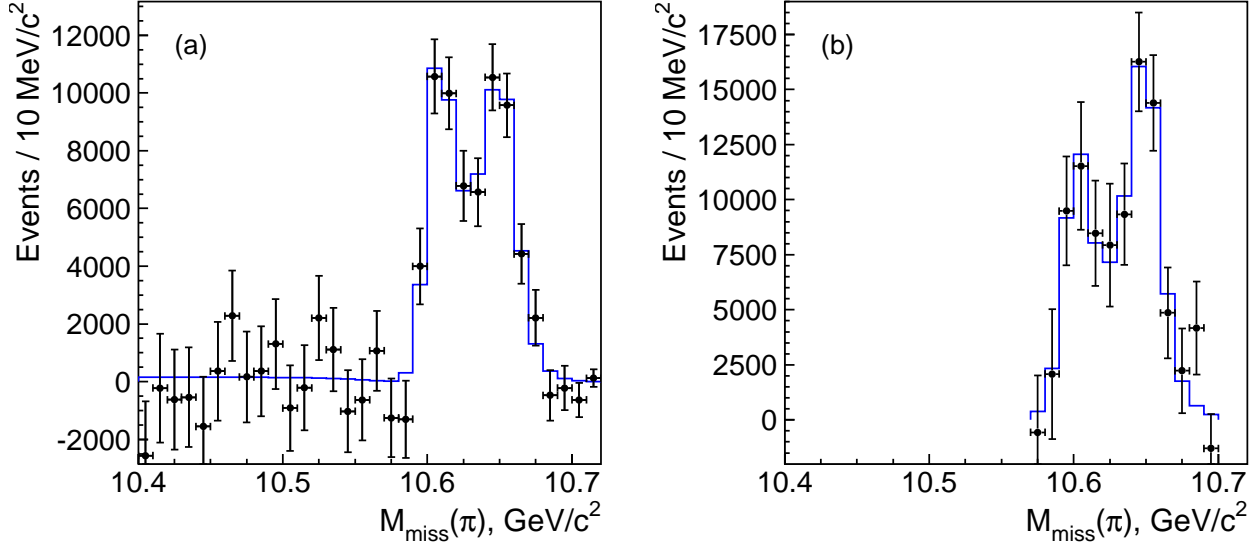


FIG. 7: The yield (dots with error bars) of (a) $h_b(1P)$ and (b) $h_b(2P)$, as a function of $M_r(\pi)$. The solid histogram shows the results of the fit.

Wigner amplitudes and a non-resonant contribution:

$$|BW_1(s, M_1, \Gamma_1) + ae^{i\phi}BW_1(s, M_2, \Gamma_2) + be^{i\psi}|^2 \frac{qP}{\sqrt{s}}, \quad (5)$$

where $\sqrt{s} \equiv M_r(\pi)$; the variables M_k, Γ_k ($k = 1, 2$), a, ϕ, b and ψ are free parameters; $\frac{qP}{\sqrt{s}}$ is a phase-space factor, where p (q) is the momentum of the pion originating from the $\Upsilon(10860)$ (Z_b) decay measured in the rest frame of the corresponding mother particle. The P -wave Breit-Wigner amplitude is expressed as $BW_1(s, M, \Gamma) = \frac{\sqrt{M\Gamma} F(q/q_0)}{M^2 - s - iM\Gamma}$, where F is the P -wave Blatt-Weisskopf form factor $F = \sqrt{\frac{1+(q_0R)^2}{1+(qR)^2}}$ [15], q_0 is the daughter momentum calculated using the pole mass of its mother, $R = 1.6 \text{ GeV}^{-1}$. The function in Eq. (5) is convolved with the detector resolution function ($\sigma = 5.2 \text{ MeV}/c^2$), integrated over the histogram bin and corrected for the reconstruction efficiency. The result of the fit is shown in Fig. 7; fractions of individual amplitudes are given in Table III.

The non-resonant contribution in the $h_b(1P)\pi^+\pi^-$ final state is found to be consistent with zero, $b = 0.18_{-0.56}^{+0.22}$ with the central value for its fit fraction of only 3.2% and an upper limit of 22% at 95% C.L. This is in accordance with the expectation that the non-resonant amplitude is suppressed due to the heavy quark spin flip. In the $h_b(1P)\pi^+\pi^-$ final state, we are not sensitive to the non-resonant amplitude due to the limited phase space and thus fixed the non-resonant component at zero.

To estimate the systematic uncertainty we vary the order of the Chebyshev polynomial in the fits to the $M_r(\pi^+\pi^-)$ spectra. To study the effect of finite $M_r(\pi)$ binning, we shift the binning by half of the bin size. To study the model uncertainty in the fits to the $M_r(\pi)$ distributions, we remove (add) the non-resonant contribution in the $h_b(1P)$ ($h_b(2P)$) case. We also vary the R parameter of the Blatt-Weisskopf form factor in the range of $0 - 5 \text{ GeV}^{-1}$ (default value is 1.6 GeV^{-1}) and find the associated systematic effect to be negligible. In Ref. [2], we find that the resolution in data could be larger than in MC by typically 10%; we increase the width of the resolution function by 10% to account for possible

TABLE III: Fit fractions of various components in three-body $\Upsilon(10860) \rightarrow h_b(mP)\pi^+\pi^-$ signals.

	$h_b(1P)\pi^+\pi^-$	$h_b(2P)\pi^+\pi^-$
non-resonant	3.2% (< 22% at 90% C.L.)	–
$Z_b(10610)\pi^\pm$	$(42.3^{+9.5}_{-12.7} \ ^{+6.7}_{-0.8})\%$	$(35.2^{+15.6}_{-9.4} \ ^{+0.1}_{-13.4})\%$
$Z_b(10650)\pi^\pm$	$(60.2^{+10.3}_{-21.1} \ ^{+4.1}_{-3.8})\%$	$(64.8^{+15.2}_{-11.4} \ ^{+6.7}_{-15.5})\%$

difference between data and MC simulation. The maximum change of parameters for each source is used as an estimate of its associated systematic error. All systematic uncertainty contributions have been added in quadrature to obtain the total systematic uncertainty.

RESULTS

To calculate branching fractions for the observed three-body $\Upsilon(10860) \rightarrow BB^*\pi$ and $\Upsilon(10860) \rightarrow B^*B^*\pi$ signals, one needs to account for the non-uniform distribution of signal events over the phase space. The corrected efficiencies are found to be $12.25 \pm 0.06\%$ and $11.0 \pm 0.1\%$, for the $\Upsilon(10860) \rightarrow BB^*\pi$ and $\Upsilon(10860) \rightarrow B^*B^*\pi$ modes, respectively. The three-body branching fractions are then calculated as

$$\mathcal{B}(\Upsilon(10860) \rightarrow B^{(*)}B^{(*)}\pi) = \frac{N_{B^{(*)}B^{(*)}\pi}}{L \cdot \sigma(e^+e^- \rightarrow \Upsilon(10860)) \cdot \mathcal{B}(B \rightarrow f) \cdot \varepsilon_{B^{(*)}B^{(*)}\pi} \cdot \alpha},$$

where $L = 121.4 \text{ fb}^{-1}$ is the total integrated luminosity and $\sigma(e^+e^- \rightarrow \Upsilon(10860)) = 0.340 \pm 0.016 \text{ nb}$ [9] is the cross section of e^+e^- annihilation into the $\Upsilon(10860)$ state at a c.m. energy of 10865 MeV. Using world average results for the secondary branching fractions [8], the combined fraction of B meson decays to all reconstructed final states including secondary branching fractions is found to be $\mathcal{B}(B \rightarrow f) = (143 \pm 15) \times 10^{-5}$ (neutral and charged B combined). Finally, one also needs to correct for the oscillation of neutral B mesons. After time integration, the fraction of oscillated neutral B mesons is equal to $f_{\text{osc}} = 0.19$. The correction factor α is calculated as:

$$\alpha = \frac{\mathcal{B}(B^+ \rightarrow f^+) \cdot \varepsilon_{B^{(*)}B^{(*)}\pi} + \mathcal{B}(B^0 \rightarrow f^0) \cdot \varepsilon_{B^{(*)}B^{(*)}\pi}(1 - f_{\text{osc}})}{\mathcal{B}(B^+ \rightarrow f^+) \cdot \varepsilon_{B^{(*)}B^{(*)}\pi} + \mathcal{B}(B^0 \rightarrow f^0) \cdot \varepsilon_{B^{(*)}B^{(*)}\pi}},$$

where $\mathcal{B}(B^+ \rightarrow f^+)$ and $\mathcal{B}(B^0 \rightarrow f^0)$ are the total fractions of B decays to charged and neutral final states (including secondary fractions), respectively. From signal MC, one gets $\alpha = 0.8978$. This results in $\mathcal{B}(\Upsilon(10860) \rightarrow BB^*\pi) = (28.3 \pm 2.9 \pm 4.6) \times 10^{-3}$ and $\mathcal{B}(\Upsilon(10860) \rightarrow B^*B^*\pi) = (14.1 \pm 1.9 \pm 2.4) \times 10^{-3}$. For the $\Upsilon(10860) \rightarrow BB\pi$ decay, we calculate a 90% confidence level upper limit of $\mathcal{B}(\Upsilon(10860) \rightarrow BB\pi) < 4.0 \times 10^{-3}$ (including systematic uncertainty).

The dominant sources of systematic uncertainties for the three-body branching fractions are the uncertainties in the secondary branching fractions, the uncertainty in the reconstruction efficiency and in the signal yield extraction and the uncertainty in the $\sigma(e^+e^- \rightarrow \Upsilon(10860))$ cross section. The overall systematic uncertainties for the three-body branching fraction are estimated to be 17.5%, 16.3% and 16.9% for the $BB\pi$, $BB^*\pi$ and $B^*B^*\pi$ final states, respectively.

TABLE IV: Results on three-body $\Upsilon(10860) \rightarrow \Upsilon(nS)\pi^+\pi^-$ branching fractions.

Final state	$\Upsilon(1S)\pi^+\pi^-$	$\Upsilon(2S)\pi^+\pi^-$	$\Upsilon(3S)\pi^+\pi^-$
Signal Yield	2090 ± 73	2476 ± 97	628 ± 41
Efficiency, %	45.9	39.0	24.4
$B(\Upsilon(nS) \rightarrow \mu^+\mu^-)$ [8], %	2.48 ± 0.05	1.93 ± 0.17	2.18 ± 0.21
$B(\Upsilon(10860) \rightarrow f)$, 10^{-3}	$4.45 \pm 0.16 \pm 0.35$	$7.97 \pm 0.31 \pm 0.96$	$2.88 \pm 0.19 \pm 0.36$
From Ref. [13], 10^{-3}	$5.3 \pm 0.3 \pm 0.5$	$7.8 \pm 0.6 \pm 1.1$	$4.8_{-1.5}^{+1.8} \pm 0.7$

The branching fractions of the three-body $\Upsilon(10860) \rightarrow \Upsilon(nS)\pi^+\pi^-$ decays are calculated with the following formula:

$$\mathcal{B}(\Upsilon(10860) \rightarrow \Upsilon(nS)\pi^+\pi^-) = \frac{N_{\Upsilon(nS)\pi^+\pi^-}}{L \cdot \sigma(e^+e^- \rightarrow \Upsilon(10860)) \cdot \mathcal{B}(\Upsilon(nS) \rightarrow \mu^+\mu^-) \cdot \varepsilon_{\Upsilon(nS)\pi^+\pi^-}}.$$

The reconstruction efficiencies (including trigger efficiency) $\varepsilon_{\Upsilon(nS)\pi^+\pi^-}$ are determined from the signal MC, $\Upsilon(nS) \rightarrow \mu^+\mu^-$ fractions [8]; the final results are given in Table IV. In determination of the reconstruction efficiencies, we use signal MC events generated according to the results of the Dalitz fit with the nominal model. The main systematic uncertainties in three-body fractions come from the $\sigma(e^+e^- \rightarrow \Upsilon(10860))$ cross section (4.7% for all channels), the $\Upsilon(nS) \rightarrow \mu^+\mu^-$ branching fractions (2.0%, 8.8% and 9.6% for $n = 1, 2, 3$, respectively), the $\Upsilon(nS)$ signal yield (4.5%, 5.3% and 4.9% for $n = 1, 2, 3$, respectively), and the MC tracking efficiency of 4% for all channels. The overall systematic uncertainty is 7.9%/12.0%/12.4% for $\Upsilon(1S/2S/3S)\pi^+\pi^-$, respectively. The results for the $\Upsilon(10860) \rightarrow \Upsilon(nS)\pi^+\pi^-$ fractions are to be compared with previous measurements by Belle with a data sample of 21 fb^{-1} [13] (see Table IV). We find the two sets of measurements to be consistent within uncertainties.

Using results of the fit to the $M_r(\pi)$ spectra with the nominal model (see Table I) and the results of the analysis of the $\Upsilon(10860) \rightarrow \Upsilon(nS)$, $n = 1, 2, 3$ and $\Upsilon(10860) \rightarrow h_b(mP)$,

 TABLE V: List of branching fractions for the $Z_b^+(10610)$ and $Z_b^+(10650)$ decays.

Channel	Fraction, %	
	$Z_b(10610)$	$Z_b(10650)$
$\Upsilon(1S)\pi^+$	0.32 ± 0.09	0.24 ± 0.07
$\Upsilon(2S)\pi^+$	4.38 ± 1.21	2.40 ± 0.63
$\Upsilon(3S)\pi^+$	2.15 ± 0.56	1.64 ± 0.40
$h_b(1P)\pi^+$	2.81 ± 1.10	7.43 ± 2.70
$h_b(2P)\pi^+$	4.34 ± 2.07	14.8 ± 6.22
$B^+\bar{B}^{*0} + \bar{B}^0B^{*+}$	86.0 ± 3.6	—
$B^{*+}\bar{B}^{*0}$	—	73.4 ± 7.0

$m = 1, 2$ decays, one can measure the ratio of the branching fractions:

$$\frac{\mathcal{B}(Z_b(10610) \rightarrow BB^*)}{\sum_n \mathcal{B}(Z_b(10610) \rightarrow \Upsilon(nS)\pi) + \sum_m \mathcal{B}(Z_b(10610) \rightarrow h_b(mP))} = 6.2 \pm 0.7 \pm 1.3_{-1.8}^{+0.0}$$

and

$$\frac{\mathcal{B}(Z_b(10650) \rightarrow B^*B^*)}{\sum_n \mathcal{B}(Z_b(10650) \rightarrow \Upsilon(nS)\pi) + \sum_m \mathcal{B}(Z_b(10650) \rightarrow h_b(mP))} = 2.8 \pm 0.4 \pm 0.6_{-0.4}^{+0.0}.$$

We also find it useful to calculate the relative fractions for Z_b decays assuming that they are saturated by the already observed $\Upsilon(nS)$ ($n = 1, 2, 3$), $h_b(mP)$ ($m = 1, 2$), and $B^*B^{(*)}$ channels. The results are summarized in Table V. We do not include the $Z_b(10650) \rightarrow BB^*$ channel in the table as this decay mode has marginal significance. However, if the central value is used, its fraction would be $25.4 \pm 10.2\%$. All other fractions would be reduced by a factor of 1.33.

Acknowledgments

We thank the KEKB group for the excellent operation of the accelerator; the KEK cryogenics group for the efficient operation of the solenoid; and the KEK computer group, the National Institute of Informatics, and the PNNL/EMSL computing group for valuable computing and SINET4 network support. We acknowledge support from the Ministry of Education, Culture, Sports, Science, and Technology (MEXT) of Japan, the Japan Society for the Promotion of Science (JSPS), and the Tau-Lepton Physics Research Center of Nagoya University; the Australian Research Council and the Australian Department of Industry, Innovation, Science and Research; the National Natural Science Foundation of China under contract No. 10575109, 10775142, 10875115 and 10825524; the Ministry of Education, Youth and Sports of the Czech Republic under contract No. LA10033 and MSM0021620859; the Department of Science and Technology of India; the Istituto Nazionale di Fisica Nucleare of Italy; the BK21 and WCU program of the Ministry Education Science and Technology, National Research Foundation of Korea, and GSDC of the Korea Institute of Science and Technology Information; the Polish Ministry of Science and Higher Education; the Ministry of Education and Science of the Russian Federation, the Russian Federal Agency for Atomic Energy and the Russian Foundation for Basic Research Grant RFBR 12-02-01296; the Slovenian Research Agency; the Swiss National Science Foundation; the National Science Council and the Ministry of Education of Taiwan; and the U.S. Department of Energy and the National Science Foundation. This work is supported by a Grant-in-Aid from MEXT for Science Research in a Priority Area (“New Development of Flavor Physics”), and from JSPS for Creative Scientific Research (“Evolution of Tau-lepton Physics”).

-
- [1] A. Bondar, A. Garmash, R. Mizuk, D. Santel, K. Kinoshita *et al.* (Belle Collaboration), Phys. Rev. Lett. **108**, 122001 (2012); I. Adachi *et al.* (Belle Collaboration), arXiv:1105.4583 [hep-ex].
 - [2] I. Adachi *et al.* (Belle Collaboration), Phys. Rev. Lett. **108**, 032001 (2012).
 - [3] A.E. Bondar, A. Garmash, A.I. Milstein, R. Mizuk, M.B. Voloshin, Phys. Rev. D **84**, 054010 (2011).

- [4] A. Drutskoy *et al.* (Belle Collaboration), Phys. Rev. **D81**, 112003 (2010).
- [5] A. Abashian *et al.*, Nucl. Instr. and Meth. **A479**, 117 (2002).
- [6] S. Kurokawa, Nucl. Instr. and Meth. **A499**, 1 (2003).
- [7] R. Brun *et al.*, GEANT 3.21, CERN Report DD/EE/84-1, 1984.
- [8] J. Beringer *et al.* (Particle Data Group), Phys. Rev. D **86**, 010001 (2012).
- [9] S. Esen, A. J. Schwarz *et al.* (Belle Collaboration), [arXiv: 1208.0323]. To be submitted to PRL.
- [10] A. Garmash *et al.* (Belle Collaboration), Phys. Rev. Lett. **96**, 251803 (2006).
- [11] M. B. Voloshin, Phys. Rev. D **74**, 054022 (2006).
- [12] M. B. Voloshin, Prog. Part. Nucl. Phys. **61**, 455 (2008).
- [13] K.-F. Chen, W.-S. Hou, M. Shapkin, A. Sokolov *et al.* (Belle Collaboration), Phys. Rev. Lett. **100**, 112001 (2008).
- [14] G.C. Fox and S. Wolfram, Phys. Rev. Lett. **41**, 1581 (1978).
- [15] J. Blatt and V. Weisskopf, Theoretical Nuclear Physics, p.361, New York: John Wiley & Sons (1952).